PHYSICAL REVIEW B VOLUME 43, NUMBER 2 15 JANUARY 1991-I

Integral-equation approach to medium-range order in molten and glassy chalcogenides

H. Iyetomi,* P. Vashishta,† and R. K. Kalia†
Materials Science Division, Argonne National Laboratory, Argonne, Illinois 60439
(Received 17 July 1989; revised manuscript received 27 June 1990)

The first sharp diffraction peak (FSDP), a signature of medium-range order in molten and vitreous chalcogenides, is investigated using the integral-equation method. A variety of interatomic potentials, including uncharged and charged hard spheres, and realistic two-body interactions, are used in this study. The two-body potential consists of steric repulsions, Coulomb interactions due to charge-transfer effects, and the effects of electronic polarizability of ions. $GeSe_2$ is treated as a specific example. The FSDP is observed in both the charged-hard-sphere and the realistic two-body interaction models. In both models steric and charge-transfer effects are found to give rise to $Ge(Se_{1/2})_4$ tetrahedra whose packing determines the medium-range order and the attendant FSDP. From the charge-charge structure factor it is found that the FSDP arises from spatial correlations where charge neutrality prevails. The nature of the medium-range correlation is elucidated through the temperature and density dependence of the FSDP and the thermal expansion determined from the shifts of the peaks in the static structure factor. We have also studied the effects of the potential parameters on the position of the FSDP. The results of the hypernetted-chain theory are compared with the molecular-dynamics results.

I. INTRODUCTION

A number of x-ray[1-3] and neutron[4-6] diffraction measurements on molten and glassy $GeSe_2$ have been carried out over the past several years. These scattering experiments clearly show the first sharp diffraction peak (FSDP) around $q=1$ Å^{-1}, which reflects the existence of medium-range correlations extending beyond the nearest-neighbor distances. Many other oxide and chalcogenide glasses such as SiO_2, GeO_2, $SiSe_2$, GeS_2 and As_2Se_3 also exhibit the medium-range order signified by the FSDP.[7,8] In addition, the FSDP of the vitreous $GeSe_2$ behaves anomalously with temperature: the peak grows as the temperature is increased in a totally reversible manner.[4]

Phillips[9] has proposed a raft model to describe the atomistic-scale structure of amorphous $GeSe_2$. In his model the interlayer correlations, similar to those in the crystalline $GeSe_2$, are responsible for the FSDP. To obtain a unified point of view for the medium-range order, Moss and Price[7] have proposed a random packing model of structural units in the context of the continuous random network model; the building unit in $GeSe_2$ is a $Ge(Se_{1/2})_4$ tetrahedron. It has not been possible, however, to determine experimentally the partial correlations and the corresponding length scales which give rise to the FSDP. The recent x-ray measurement by Fuoss and Fischer-Colbrie[3] on thin films of amorphous $GeSe_2$ gave no evidence for low-dimensional correlations; i.e., the x-ray pattern did not change with sample thickness.

A recent molecular-dynamics (MD) study of molten and glassy $GeSe_2$ by Vashishta *et al.*[10,11] has shed light on the structural and dynamical properties of chalcogenide glasses. The MD results manifest the formation of a network structure composed of $Ge(Se_{1/2})_4$ tetrahedra. The effective potential in the MD study consists of (i) the steric repulsion described by a power-law interaction, (ii) the long-ranged Coulomb interaction stemming from charge transfer between Ge and Se, (iii) the charge-dipole interaction due to the large electronic polarizability of seleniums, and (iv) three-body forces accounting for the covalent nature of the bonding.

The MD calculation indicates that the constrained space-filling of atoms, subject to the excluded-volume effect and local charge neutrality, can give rise to medium-range order associated with the FSDP. In this paper we therefore study the steric and charge-transfer effects systematically and elucidate the physical nature of the intermediate-range correlation at the level of interatomic potentials.

The following models for $GeSe_2$ are considered: (a) the mixture of neutral hard spheres, (b) the mixture of charged hard spheres, and (c) a system with the effective potential due to Vashishta *et al.*[10,11] The essential features of the excluded-volume effect and the local charge neutrality are incorporated in model (b). In the present study with model (c) we take into account only the two-body contributions, although three-body and higher-order interactions may be important in reproducing certain kinds of structural correlations in covalent materials. The MD study[10] of AX_2-type systems demonstrates that all the properties of these glasses can be accounted for by two-body interactions in a semiquantitative manner. This is partly because tetrahedral coordination in AX_2-type systems is possible in the context of only pairwise interactions. The discrepancies between the two-body and experimental results, such as the disagreement in the position of the FSDP in $GeSe_2$, are a

manifestation of three-body forces which cannot be renormalized entirely in a two-body form.[11] For monatomic systems the situation is quite different. Three-body forces have to be explicitly incorporated for a satisfactory description of pure elemental semiconductors such as Si and Ge. No reasonable two-body potential indeed stabilizes the diamond structure in these systems against close-packed structures.[12,13]

To calculate the structural correlation functions we take advantage of the integral-equation method instead of the MD approach. The simplicity of the method enables us to study these systems extensively. Since the experimental results do not show[4] a qualitative difference between the static structure factors of the molten and vitreous $GeSe_2$, it is expected that the applicability of the integral-equation scheme can be carried over to the glassy states. The theoretical schemes used here are the Percus-Yevick (PY) scheme[14] for model (a) and the hypernetted-chain (HNC) scheme[15,16] for models (b) and (c). The HNC scheme accurately accounts for the long-range Coulombic interaction.[17]

The anomalous temperature dependence of the FSDP is then studied by taking into account the increase in the number density on cooling. The actual temperature dependence is divided into two contributions: the temperature-induced change at constant density and the density-induced change at constant temperature. The analysis of thermal expansion through the shifts of the peaks in the static structure factor provides additional insight into the properties of intermediate-range correlations. A detailed comparison of the theoretical and experimental values for the position of the FSDP assesses the importance of three-body covalent forces. We also examine the accuracy of the HNC approximation in predicting the thermodynamic quantities by comparing it with the MD results. This is important for future studies of structural properties of more complicated ternary systems such as Ag/Ge/Se.[18] Brief and preliminary accounts of the present study have been reported elsewhere.[19,20]

In Sec. II we first define the three models considered here by specifying the interaction potentials. A brief account of the integral-equation schemes for the correlation functions is given in Sec. III. Section IV is devoted to discussion of the results. The main conclusions are summarized in Sec. V.

II. INTERATOMIC POTENTIALS

The effective pair potential for $GeSe_2$ proposed by Vashishta *et al.*[10] consists of three terms: the Coulomb interaction, charge-dipole interaction, and steric repulsion. The explicit form for the potential between atoms of μ and ν species of is

$$\phi_{\mu\nu}(r)=\frac{Z_\mu Z_\nu}{r}-\frac{\frac{1}{2}(\alpha_\mu Z_\nu^2+\alpha_\nu Z_\mu^2)}{r^4}e^{-r/r_{4s}}+\frac{H_{\mu\nu}}{r^{\eta_{\mu\nu}}} . \quad (1)$$

Here Ge and Se atoms are assumed to have effective charges of $4Z+$ and $2Z-$, respectively; Z is chosen to be $0.33e$. The other parameters involved in Eq. (1) are listed below:

$$\alpha_{Ge}=0, \quad \alpha_{Se}=7.0, \quad r_{4s}=4.43 ,$$
$$H_{Ge\text{-}Ge}=1.114, \quad H_{Ge\text{-}Se}=146.1, \quad H_{Se\text{-}Se}=284.1 , \quad (2)$$
$$\eta_{Ge\text{-}Ge}=11, \quad \eta_{Ge\text{-}Se}=9, \quad \eta_{Se\text{-}Se}=7 ,$$

where the length and energy are measured in units of Å and $e^2/$Å ($=14.40$ eV), respectively. The interaction potential, Eq. (1), with the constants given in Eq. (2) defines model (c).

The potential for the charged-hard-sphere mixture, model (b), is defined as

$$\phi_{\mu\nu}(r)=\begin{cases}\infty & \text{for } r<\sigma_\mu+\sigma_\nu \\ Z_\mu Z_\nu/r & \text{for } r>\sigma_\mu+\sigma_\nu,\end{cases} \quad (3)$$

where the effective charges Z_μ were taken to be the same as those in the effective potential, Eq. (1). The ionic radii σ_μ were determined from the bond lengths of Ge-Se (2.35 Å) and Se-Se (3.75 Å) in the glassy[2,4–6] and crystalline[21] states: $\sigma_{Ge}=0.475$ Å and $\sigma_{Se}=1.875$ Å. The potential for the neutral hard-sphere system, model (a), is given by neglecting the Coulomb interaction in Eq. (3), i.e., $Z_\mu=0$. The pair potentials $\phi_{\mu\nu}(r)$ in the three models for $GeSe_2$ are shown in Fig. 1.

III. INTEGRAL-EQUATION SCHEMES

The exact equation for $g_{\mu\nu}(r)$ of the system at temperature T can be written as

$$g_{\mu\nu}(r)=\exp[-\phi_{\mu\nu}(r)/k_BT+h_{\mu\nu}(r)-c_{\mu\nu}(r)+B_{\mu\nu}(r)] . \quad (4)$$

Here the direct correlation functions $c_{\mu\nu}(r)$ are related to the total pair-correlation functions $h_{\mu\nu}(r)=g_{\mu\nu}(r)-1$

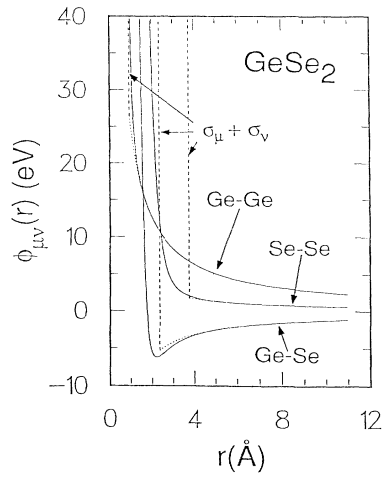

FIG. 1. Pair potentials $\phi_{\mu\nu}(r)$ in the three models for $GeSe_2$. Three solid curves are from Eqs. (1) and (2), and define the model (c). Three vertical dashed lines show hard-sphere repulsions at $\sigma_\mu+\sigma_\nu$; the joining dotted lines are for the Coulomb interactions. Model (b) includes the hard-sphere repulsions and Coulomb interactions, whereas model (a) has only the hard-sphere repulsions.

through the Ornstein-Zernike relation

$$h_{\mu\nu}(r)=c_{\mu\nu}(r)+\sum_{\beta}\rho_{\beta}\int d\mathbf{r}_1 c_{\mu\beta}(|\mathbf{r}-\mathbf{r}_1|)h_{\beta\nu}(r_1)\ , \tag{5}$$

where ρ_β is the number density of the β-species atoms. Equations (4) and (5) were originally derived[15,22] by infinite summation of the cluster-expansion diagrams; the formulation based on the density-functional theory gives an alternative derivation of those equations.[23]

The HNC equation[15,16] is obtained by neglecting the bridge-diagram contribution $B_{\mu\nu}(r)$ in Eq. (4):

$$g_{\mu\nu}(r)=\exp[-\phi_{\mu\nu}(r)/k_BT+h_{\mu\nu}(r)-c_{\mu\nu}(r)]\ . \tag{6}$$

The linearization of the HNC equation (6) with respect to the nodal functions

$$\gamma_{\mu\nu}(r)=h_{\mu\nu}(r)-c_{\mu\nu}(r) \tag{7}$$

results in the PY equation,[14]

$$g_{\mu\nu}(r)=\exp[-\phi_{\mu\nu}(r)/k_BT][1+\gamma_{\mu\nu}(r)]\ . \tag{8}$$

The HNC or PY equation and the Ornstein-Zernike relation constitute a closed set of equations for the correlation functions.

It is widely known[22,24] that for hard spheres the solutions of the HNC equation are less accurate than the PY results; the higher-order terms in $\gamma_{\mu\nu}(r)$ are fortuitously canceled out by the bridge-diagram contributions. On the other hand, for systems with Coulomb interactions, the HNC theory is much superior to the PY theory.[23,25] Recently the interrelationship among the HNC approximation, the convolution approximation for the correlation functions, and the charge neutrality conditions has been elucidated theoretically;[17] the HNC approximation takes accurate account of the long-ranged nature of the Coulomb interaction.

Analytic solutions to the PY equation are available for hard-sphere systems.[26–31] In contrast, the HNC equation must be solved numerically. To handle the numerical instability caused by the attractive part of the potential between Ge and Se atoms, we utilize the efficient Newton-Raphson technique according to Gillan's prescription;[32] formal generalization of his method to multicomponent systems was carried out by Enciso.[33]

The key idea is to decompose the correlation functions into the coarse-grained contributions and the remaining into fine contributions. The coarse-grained contributions, spanned by a small number of basis functions, are determined by the Newton-Raphson method, while the fine contributions, which are expected to have a small influence on the convergence, are calculated by a simple iterative method. The advantage of this method lies not only in its rapid convergence but also in its insensitivity to initial conditions.[32] In addition, the long-range problem posed by the Coulomb interaction was solved with Ng's method.[34]

We can express the excess internal energy and pressure in terms of the correlation functions using the standard thermodynamic relations:

$$U/N=\tfrac{1}{2}\sum_{\mu\nu}x_\mu x_\nu\rho\int d\mathbf{r}\,\phi_{\mu\nu}(r)g_{\mu\nu}(r)\ , \tag{9}$$

$$P/\rho=-\tfrac{1}{6}\sum_{\mu\nu}x_\mu x_\nu\rho\int d\mathbf{r}\,r\frac{\partial\phi_{\mu\nu}(r)}{\partial r}g_{\mu\nu}(r)\ , \tag{10}$$

where N, ρ, and x_μ denote the total number of atoms, the total number density, and the concentration of atoms of species μ, respectively. The HNC scheme has a unique feature in that the excess chemical potential and hence the excess Helmholtz free energy can be calculated directly from the correlation functions:[16,25]

$$\mu_\nu/k_BT=\sum_{\mu}x_\mu\left[\frac{\rho}{2}\int d\mathbf{r}\,h_{\mu\nu}(r)\gamma_{\mu\nu}(r)-\frac{\rho}{2}\int d\mathbf{r}\,c^R_{\mu\nu}(r)\right]\ , \tag{11}$$

$$F/N=\sum_{\nu}x_\nu\mu_\nu-P/\rho\ . \tag{12}$$

Here $c^R_{\mu\nu}$ is a regular part of the direct correlation functions $c_{\mu\nu}$ defined as

$$c^R_{\mu\nu}(r)=c_{\mu\nu}(r)+\frac{Z_\mu Z_\nu}{rk_BT}\ . \tag{13}$$

IV. RESULTS AND DISCUSSION

For the purpose of the numerical computations, the range of r is divided into a set of N equal mesh points $r_i=(i-1)\Delta r$ $(i=1-N)$. Then the functions $\gamma_{\mu\nu}(r)$, etc., are represented by their values $\gamma_{\mu\nu}(i)=\gamma_{\mu\nu}(r_i)$, etc., on these positions. The number N of mesh points and the increment Δr taken in the present calculations are $N=1024$ and $\Delta r=0.05a$ with $a=(3/4\pi\rho)^{1/3}$. The Fourier transformations were calculated with a fast Fourier transform (FFT) algorithm; the interval Δq of the wave number is related[35] to Δr through

$$\Delta q=\pi/N\Delta r\ . \tag{14}$$

To obtain converged solutions to the HNC equation, we were compelled to start at a very high temperature (e.g., $T=10\,000$ K) with a given density ($\rho=3.114\times10^{22}$ cm^{-3} for the liquids or $\rho=3.443\times10^{22}$ cm^{-3} for the glasses).[6] Then we reduced the temperature step by step with the density kept constant; the solution is sensitive to the density change. At each new step in this procedure we used as input the nodal functions obtained at the previous stage. Finally, we reached $T=300$ K in model (c) with the effective potential, Eq. (1), and $T=1071$ K in model (b) with the charged-hard-sphere potential, Eq. (2).

The partial static structure factors $S_{\mu\nu}(q)$ are calculated from the Fourier transforms of the corresponding pair-distribution functions through

$$S_{\mu\nu}(q)=\delta_{\mu\nu}+4\pi(\rho_\mu\rho_\nu)^{1/2}\int_0^\infty dr\,r^2[g_{\mu\nu}(r)-1]\frac{\sin(qr)}{qr}\ . \tag{15}$$

The density-density structure factor $S_{\rho\rho}(q)$ and the charge-charge structure factor $S_{ZZ}(q)$ are then obtained by taking appropriate linear combinations of $S_{\mu\nu}(q)$:

$$S_{\rho\rho}(q)=\sum_{\mu\nu}(x_\mu x_\nu)^{1/2}S_{\mu\nu}(q)\ , \tag{16}$$

$$S_{ZZ}(q)=\frac{1}{\langle Z^2\rangle}\sum_{\mu\nu}Z_\mu Z_\nu(x_\mu x_\nu)^{1/2}S_{\mu\nu}(q)\ , \tag{17}$$

where $\langle Z^2\rangle=\sum_\mu x_\mu Z_\mu^2$. Since Ge atoms have a coherent scattering length ($b_{\rm Ge}=0.819\times10^{-12}$ cm) that is very close to that of Se atoms ($b_{\rm Se}=0.797\times10^{-12}$ cm), the structure factor[36] measured by the neutron diffraction experiment,

$$S_n(q)=\frac{\sum_{\mu\nu}b_\mu b_\nu(x_\mu x_\nu)^{1/2}[S_{\mu\nu}(q)-\delta_{\mu\nu}+(x_\mu x_\nu)^{1/2}]}{\left[\sum_\mu x_\mu b_\mu\right]^2}\ , \tag{18}$$

practically reduces to $S_{\rho\rho}(q)$.

A. Short-range order, medium-range order, and charge-charge correlations

In Fig. 2 we compare the partial pair-distribution functions $g_{\mu\nu}(r)$ of the three models in the molten state at $\rho=3.114\times10^{22}$ cm^{-3} and $T=1071$ K, which is just above the melting point of $GeSe_2$, $T=1015\pm2$ K.[37] The coordination numbers associated with $g_{\mu\nu}(r)$ are also marked in Fig. 2. The coordination number $N_{\mu\nu}(R)$ of the νth species around an atom of μ species is obtained by integrating the corresponding partial pair-distribution function $g_{\mu\nu}(r)$ as

$$N_{\mu\nu}(R)=4\pi\rho_\nu\int_0^R dr\, r^2 g_{\mu\nu}(r)\ . \tag{19}$$

The distance R defines the first coordination shell, which was chosen to coincide with the first minimum in $g_{\mu\nu}(r)$.

Figure 2 shows that all the three models have the same

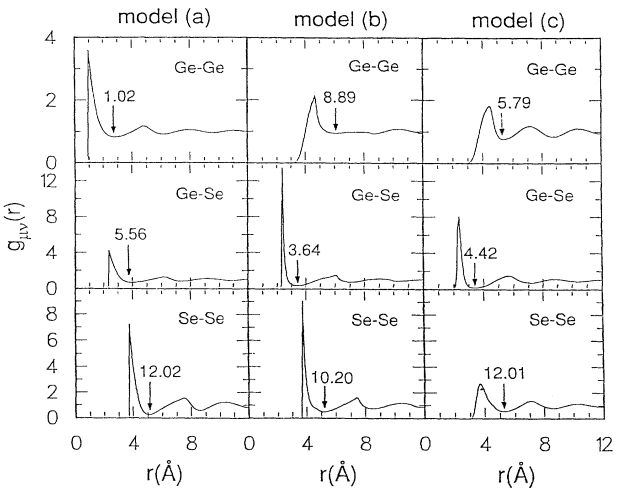

FIG. 2. Partial pair-distribution functions $g_{\mu\nu}(r)$ for the three models (a), (b), and (c) for molten $GeSe_2$ ($T=1071$ K and $\rho=3.114\times10^{22}$ cm^{-3}). The coordination numbers are marked above the arrows, which are at the minima after the first peaks.

bond lengths $d_{\mu\nu}$ for Ge-Se and Se-Se pairs, which are defined from the first peak positions in $g_{\mu\nu}(r)$: $d_{\text{Ge-Se}}\approx2.35$ Å and $d_{\text{Se-Se}}\approx3.75$ Å. In contrast, the Ge-Ge mean separation is remarkably different between the uncharged hard spheres, model (a), and charged hard spheres, model (b). The Ge atoms are well separated from each other in models (b) and (c), while $g_{\text{Ge-Ge}}(r)$ has a main peak at the Ge-Ge contact distance $2\sigma_{\rm Ge}$ in model (a).

Because the spheres are uncharged in model (a), smaller spheres can be in any of the voids created by the packing of larger spheres. This leads to the following sequence of distances: $d_{\text{Ge-Ge}}<d_{\text{Ge-Se}}<d_{\text{Se-Se}}$. Also the coordination of Ge-Ge is very low and there are hardly any shell structures. It looks like a small number of Ge distributed randomly over a large number of voids. The Ge-Ge coordination is difficult to define because of the shallowness of the minimum after the main peak, which occurs at $2\sigma_{\rm Ge}$. The Ge-Se coordination is nearly 6 and the Se-Se coordination is 12, indicating the random close packing of Se atoms.

In model (b) the Ge-Se coordination is close to 4 and sharply defined when compared to the corresponding coordination in model (a). The Se-Se bond length is $2\sigma_{\rm Se}$ and quite sharply defined with the coordination number of 10. What is important to notice is that the Ge-Ge distribution function does not start at $2\sigma_{\rm Ge}$, as in model (a), but at a distance of about $2\sigma_{\rm Se}$ and has a first peak at a separation larger than the Se-Se bond length. This is what we call conditional packing. The Coulomb attraction between Ge and Se atoms makes the Ge-Se distance well defined along with the tetrahedral coordination. The Se atoms with the larger steric size occupy most of the volume in the system so that the Se-Se distribution function has a well-defined main peak. The Ge-Ge separation is determined as a consequence of the Ge-Se and Se-Se packing, resulting in $d_{\text{Ge-Ge}}$ larger than $d_{\text{Se-Se}}$.

Model (c), based on the effective potential Eq. (1), has essentially the same effects as the steric repulsion and the Coulomb interaction in model (b). However, since it has a more realistic steric repulsion (soft sphere) and includes attractive effects due to electronic polarizability, there are differences in the detailed structure of the correlation functions between these models. The manifestation of the realistic interaction is clear in the broader principal peak of $g_{\text{Ge-Se}}(r)$ along with the coordination slightly larger than 4. In addition, the Se-Se correlation has a close-packed structure with the coordination of 12. The Ge-Ge coordination is about 6. It might be mentioned here that it is the Ge-Ge correlation which is most strongly affected by the inclusion of three-body interactions.[11]

We conclude the discussion of the partial pair-distribution functions and coordination numbers with the following observation: even though the Ge-Se and Se-Se bond lengths are about 2.35 and 3.75 Å, respectively, in all the three models (a), (b), and (c), and these two distances are consistent with the formation of $Ge(Se_{1/2})_4$ tetrahedra since $3.75/2.35\approx(8/3)^{1/2}$, $Ge(Se_{1/2})_4$ tetrahedra are formed only in charged models (b) and (c) and not

in uncharged model (a). This is mainly reflected in the Ge-Ge mean separation, which is much smaller in model (a) than in models (b) and (c).

Figure 3 shows the results for the partial structure factors $S_{\mu\nu}(q)$ calculated from $g_{\mu\nu}(r)$ in Fig. 2 through Eq. (15). The neutron structure factor $S_n(q)$, and calculated and experimental results, are shown in Fig. 4, along with the charge-charge structure factor $S_{ZZ}(q)$. All the features observed in the scattering measurements are reproduced in the realistic model (c), except for the discrepancy in the position of the FSDP. This is simply reminiscent of the recent success of the MD calculation.[10] The discrepancy in the position of the FSDP will be discussed later.

Comparing these three results for $S_n(q)$ in Fig. 4, we see that the FSDP appears at the stage of the charged-hard-sphere model (b), although the "second" and "third" peaks already exist at their correct positions even in the uncharged-hard-sphere model (a). As far as the first three peaks are concerned, the charged-hard-sphere model reproduces essential features of the correlations involved in molten $GeSe_2$; the prominent long-ranged oscillations observed in the correlation functions are artifacts of the hard-sphere steric repulsions.

It is apparent from Fig. 3 that the Ge-Ge and Ge-Se first peaks are responsible for the FSDP in $S_n(q)$. The relevance of Ge correlations to the FSDP is indicated by a series of experiments[38] on $GeTe_2$-$GeSe_2$ glasses; the replacement of Te by the weak scatterer Se enhances the Ge contribution, leading to a dramatic growth of the FSDP. This is also supported by differential anomalous x-ray scattering studies[1] of a-$GeSe_2$ near the Ge absorption edge.

In the charge-charge static structure factor $S_{ZZ}(q)$, shown by the dashed line in Figs. 4(b) and 4(c), the peaks around 2.0 Å^{-1} in $S_{\mu\nu}(q)$, being collectively combined in Eq. (17), give rise to the sharp peak. On the other hand, the FSDP's at 1.4 Å^{-1} in $S_{\text{Ge-Ge}}(q)$ and $S_{\text{Ge-Se}}(q)$ are totally canceled; only a small bump is observed. Thus it turns out that the FSDP essentially has a neutral character and is associated with correlations whose spatial extent is determined by local charge neutrality.

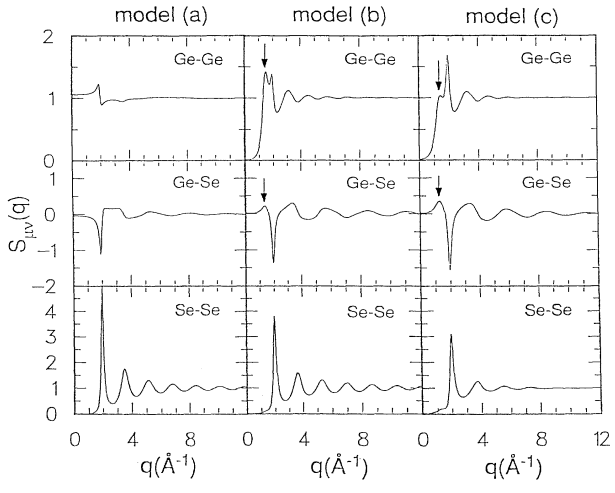

FIG. 3. Partial static structure factors $S_{\mu\nu}(q)$ associated with $g_{\mu\nu}(r)$ in Fig. 2. The arrows mark the FSDP.

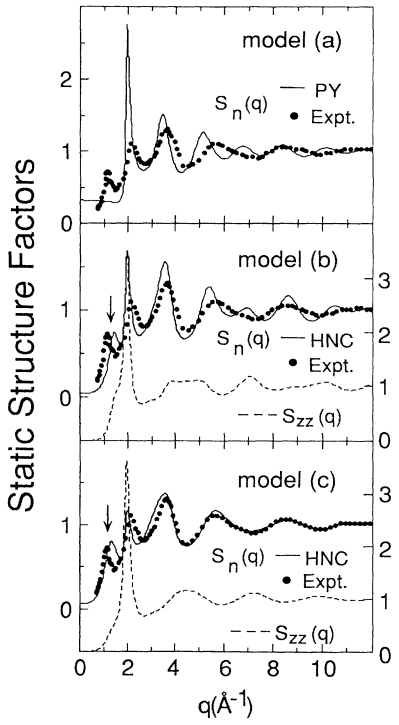

FIG. 4. Neutron-scattering structure factor $S_n(q)$ and charge-charge structure factor $S_{ZZ}(q)$ in the three models for $GeSe_2$ at the liquid density $\rho = 3.114 \times 10^{22}$ cm^{-3}. The integral-equation results [using the PY scheme in model (a) and the HNC scheme in models (b) and (c)] are shown for $S_n(q)$, solid curve, and $S_{ZZ}(q)$, dashed curve, at $T = 1071$ K. The solid circles are results from neutron-diffraction experiment[6] at $T = 1084$ K.

The medium-range correlations for Ge atoms centered at the tetrahedra can be calculated in real space from

$$\delta N_{\mu\nu}(R) = \delta_{\mu\nu} + 4\pi\rho_\nu \int_0^R dr\, r^2 [g_{\mu\nu}(r) - 1] \,. \tag{20}$$

This function, introduced by Dixon and Atwood,[39] measures how many excess atoms of the νth species are contained in a sphere of radius R with a given μ species atom at the origin. Figure 5 compares the excess numbers for Ge atoms in the neutral and charged-hard-sphere models, which were calculated using $g_{\text{Ge-Ge}}(r)$ in Fig. 2. We see that the Ge-Ge correlation in the charged-hard-sphere model is significantly enhanced in the range (≈ 10 Å), corresponding to the third peak in $g_{\text{Ge-Ge}}(r)$. On the other hand, the neutral hard spheres have no such enhancement of correlations on the scale of the intermediate-range order.

From the above results a microscopic understanding of the intimate connection between the appearance of the FSDP and the existence of basic structural units emerges. A combination of steric and Coulomb forces gives rise to

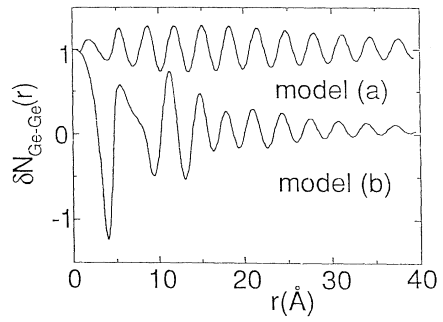

FIG. 5. Comparison of the excess number function $\delta N_{Ge\text{-}Ge}(r)$ between the (a) neutral and (b) charged hard-sphere models, based on $g_{Ge\text{-}Ge}(r)$ in Fig. 2.

$Ge(Se_{1/2})_4$ tetrahedral units where the charge of a fourfold coordinated Ge atom is locally balanced by twofold coordinated Se atoms. These neutral units form a network structure, and the correlations over distances characterized by the local charge neutrality results in the FSDP. The appearance of the FSDP thus does not depend on the minor details in the potential. This fact explains the universal occurrence of the FSDP in binary covalent glasses.

The HNC solution for the realistic model (c) was extended much below the melting temperature to $T=300$ K. Figures 6 and 7 show the results for $g_{\mu\nu}(r)$ together

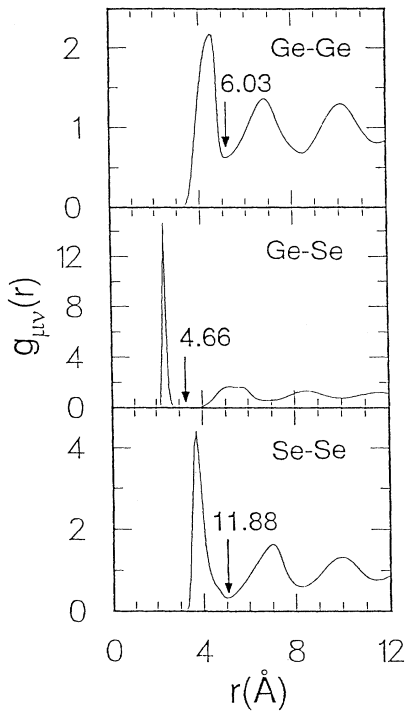

FIG. 6. Partial pair-distribution functions $g_{\mu\nu}(r)$ for vitreous $GeSe_2$ ($T=300$ K, $\rho=3.443\times10^{22}$ cm^{-3}) calculated with the effective potential Eq. (1), model (c). The coordination numbers are marked above the arrows whose positions coincide with the first minima.

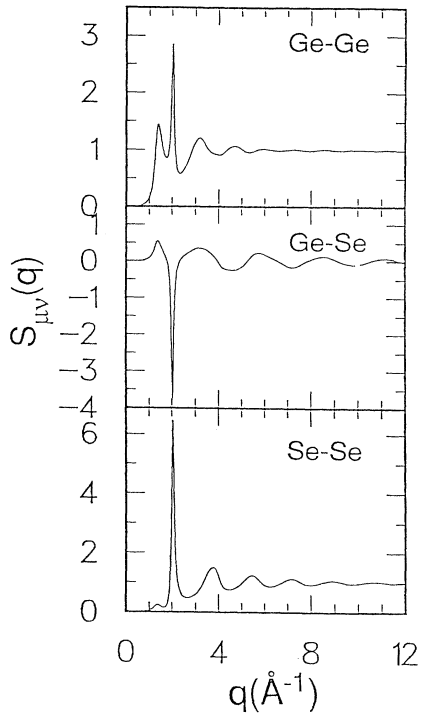

FIG. 7. Partial static structure factors $S_{\mu\nu}(q)$ associated with $g_{\mu\nu}(r)$ in Fig. 6.

with the coordination numbers and $S_{\mu\nu}(q)$ at $T=300$ K and the glass density (3.443×10^{22} cm^{-3}). Figure 8 compares the calculated $S_n(q)$ at $T=300$ K with the experimental results of vitreous $GeSe_2$ measured[6] at $T=10$ K; the results for $S_{ZZ}(q)$ are also depicted by the dashed line. We find that the HNC values for $S_n(q)$ are in good agreement with the experimental results. Even the splitting of the fourth peak into two features is observed in the HNC calculation, as Fig. 8 shows. The first peak in $S_{ZZ}(q)$ is still nothing more than a small shoulder at such a low temperature.

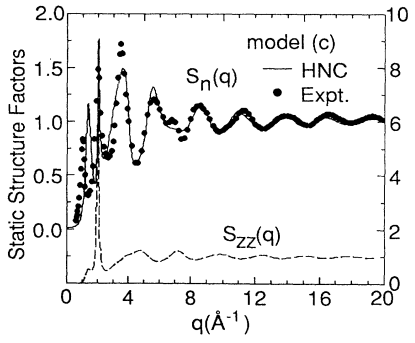

FIG. 8. Neutron-scattering structure factor $S_n(q)$ and charge-charge static structure factor $S_{ZZ}(q)$ in the vitreous $GeSe_2$. The solid and dashed curves refer to the HNC results for $S_n(q)$ and $S_{ZZ}(q)$ in model (c) at $T=300$ K. The solid circles are neutron data (Ref. 6) measured at $T=10$ K.

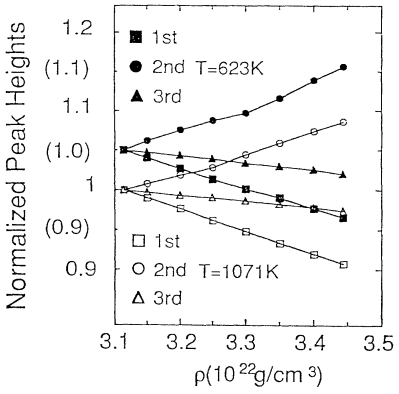

FIG. 9. Variation of the height of the first three peaks in $S_{\rho\rho}(q)$ as a function of density at fixed temperatures, based on model (c). Each peak height is normalized with the value at the liquid density (3.114×10^{22} cm^{-3}).

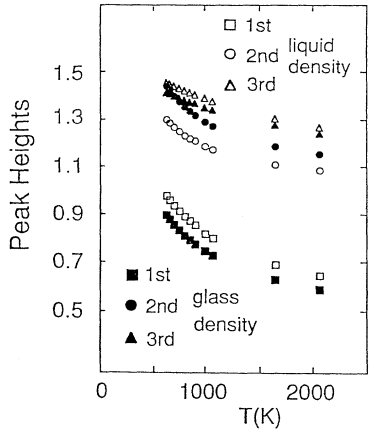

FIG. 10. Variation of height of the first three peaks in $S_{\rho\rho}(q)$ as a function of temperature at fixed densities, based on model (c).

B. Anomalous temperature dependence of the FSDP

The MD calculations reveal that the anomalous decrease in the height of the FSDP on cooling is due to frustration in the packing of the tetrahedra enhanced by the increased density;[10,11] the density also varies as a function of temperature in the experimental situation, namely, under the condition of constant pressure.

To understand the density effect, we calculated the height of the first three peaks in $S_{\rho\rho}(q)$ as a function of density at fixed temperatures and the results are shown in Fig. 9; the effective potential, as expressed in Eq. (1), was used in these calculations. The density dependence of each peak shows a different trend: the height of the FSDP decreases, the second peak increases, and the third peak shows no significant change, as the density is increased. The unusual behavior of the FSDP thus indicates that medium-range order is reduced with the increased density. This result is consistent with the recent x-ray-diffraction experiment[40] on an analogous system, namely, amorphous GeS_2: under a hydrostatic pressure (the density is accordingly increased), the height of the FSDP in a-GeS_2 is depressed. On the other hand, Fig. 10 shows that the height of all the peaks decrease with increasing temperature, as expected, at constant density.

In the HNC calculation, the depression of the FSDP with the increased density is overcome by the increase resulting from cooling alone. As a result, the FSDP does not exhibit the anomalous behavior observed experimentally. In the MD calculations,[10,11] since the density-induced change is larger than the associated change due to temperature variation, the FSDP indeed shows the anomalous behavior in agreement with the experiments.[4] This subtle cancellation of the density and temperature effects is not correctly predicted by the HNC approximation. It is mentioned once again, however, that the separate behavior of the FSDP as a function of density or temperature is described in a qualitatively correct way within the HNC approximation. It is hoped that inclusion of bridge-diagram corrections to the HNC equation (6) will improve these shortcomings.

C. Thermal-expansion coefficients

The shifts of the peak positions in $S_{\rho\rho}(q)$ as a function of temperature and density provide a different characterization of the medium-range order. Table I lists the positions of the first three peaks in $S_{\rho\rho}(q)$ calculated with the effective potential (1) for five different densities and temperatures. Clearly, the density change at constant temperature affects the FSDP much more than the peaks at higher values of q. The shift of the peak positions as a function of density at constant temperature, defined by $\Delta \ln_{10}(q)/\Delta \ln_{10}(\rho)$, is calculated to be 0.55 (0.55), 0.22 (0.20), and 0.15 (0.13) at $T=1071$ K (623 K) for the first, second, and third peaks, respectively. In addition, the position of the FSDP shifts toward a lower value of q as the temperature is decreased at constant density, while

TABLE I. Position of the first three peaks in the density-density structure factor $S_{\rho\rho}(q)$ as a function of temperature and density, based on model (c) with the effective potential Eq. (1).

T (K)	ρ (10^{22} cm^{-3})	q_1 (Å^{-1})	q_2 (Å^{-1})	q_3 (Å^{-1})
1071	3.114	1.324	1.988	3.554
1071	3.443	1.399	2.032	3.609
623	3.114	1.311	1.995	3.576
623	3.443	1.386	2.035	3.624
300	3.443	1.382	2.046	3.631

the other peaks show the opposite behavior.

This distinctive feature of the FSDP may be reflected in the thermal-expansion coefficients α, which are determined from each peak shift as

$$\alpha=-\frac{1}{q}\left[\frac{\partial q}{\partial T}\right]_P=-\frac{1}{q}\left[\frac{\partial q}{\partial T}\right]_\rho-\frac{1}{q}\left[\frac{\partial q}{\partial \rho}\right]_T\left[\frac{\partial \rho}{\partial T}\right]_P . \tag{21}$$

Experimentally the coefficients α were measured for vitreous As_2Se_3 by Busse and Nagel.[41] Their results are $\alpha=(1.2\pm0.2)\times10^{-4}$ K^{-1} and $(5.9\pm1.0)\times10^{-5}$ K^{-1} for the first and the second peaks of the static structure factor, respectively. This difference of a factor of 2 is due to different $(\partial q/\partial\rho)_T$ and it indicates that there exists two characteristic length scales distinguishing the medium-range correlations from the short-range correlations.

To evaluate α, we use finite differences to calculate Eq. (21) from the results for the liquid ($T=1071$ K and $\rho=3.114\times10^{22}$ cm^{-3}) and the glassy ($T=300$ K and $\rho=3.443\times10^{22}$ cm^{-3}) states; these two states have almost the same pressure (see Table II). This calculation gives $\alpha=6\times10^{-5}$ K^{-1} for the first peak, 4×10^{-5} K^{-1} for the second peak, and 3×10^{-5} K^{-1} for the third peak. These values agree reasonably with the experimental values, considering that the systems are different and the present calculation is crude. This result reveals another feature of the FSDP in quantitative agreement with experimental observations.

D. Location of the FSDP

As noted before, there still remains a discrepancy between the experimental and our calculated values for the position of the FSDP (1 Å^{-1} versus 1.4 Å^{-1}). The location of the FSDP in a-$GeSe_2$ has also been related to the interlayer spacing in crystalline $GeSe_2$.[9] We investigated to what extent the parameters of the charged-hard-sphere potential Eq. (2) influence the position of the FSDP. The decrease in the Se-Se contact distance from 3.75 to 3.4 Å, in fact, improves significantly the overall agreement with the experimental results, as can be seen in Fig. 11. However, the position of the FSDP is quite insensitive to this change in the Se-Se separation. Clearly, the discrepancy in the position of the FSDP is due to effects of three-body covalent interactions among atoms, which can be included in the present framework.[42] The inclusion of such forces actually modifies the connectivity between neighboring tetrahedra which, in turn, shifts the position of the FSDP to 1 Å^{-1}, in excellent agreement with diffraction measurements on amorphous and molten $GeSe_2$.[11] Fuoss and Fisher-Colbrie[3] in their synchrotron x-ray studies find no evidence of layering correlations in a-$GeSe_2$. Neutron experiments find FSDP in molten $GeSe_2$ at the same wave vector (1 Å^{-1}) as in a-$GeSe_2$.[4,6] Furthermore, in the molten and a-$GeSe_2$ the height of the FSDP is nearly the same.[6] Synchrotron x-ray studies and neutron-diffraction experiments together give strong support against the layering model.[9] In the context of the vibrational density of states, Sen and Thorpe[43] pointed out a critical role of the AXA bond angle in AX_2-type glasses, which controls the connectivity of the tetrahedral network.

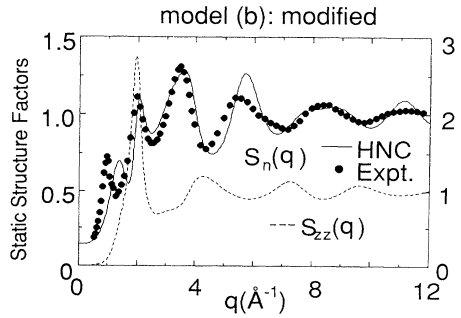

FIG. 11. Effect of varying σ_{Se} in model (b) in the HNC approximation. Solid and dashed curves refer to $S_n(q)$ and $S_{ZZ}(q)$, respectively, calculated at $T=1071$ K and $\rho=3.114\times10^{22}$ cm^{-3}, corresponding to Fig. 4(b). The Se-Se contact distance $2\sigma_{Se}$ has been changed from 3.75 to 3.4 Å.

E. Thermodynamic quantities

Table II compares the HNC results for thermodynamic quantities in the realistic model (c) with the corresponding MD results.[10] The HNC values for the internal energy are in good agreement with those of the MD calculation. On the other hand, the HNC values of the pressure are considerably different from the MD results. There exists a noticeable difference between these two calculations for the pressure. This is understandable because the

TABLE II. Excess internal energy U and pressure P calculated with the effective potential Eq. (1). HNC and MD refers to the values calculated using the hypernetted-chain scheme and the molecular-dynamics method (Ref. 10), respectively.

T (K)	ρ (10^{22} cm^{-3})	U/N (eV)		P (kbar)	
		HNC	MD	HNC	MD
1071	3.114	−4.09	−4.14	39.8	15.8
1071	3.443	−4.02	−4.07	63.7	34.1
623	3.114	−4.28		33.3	
623	3.443	−4.23	−4.20	52.4	34.2
300	3.443	−4.49	−4.30	43.3	26.0

pressure is determined from a delicate balance between large positive and negative contributions, and thus the error inherent in the HNC theory is magnified.

V. CONCLUSION

In conclusion, the physical origin of the medium-range order associated with the FSDP has been elucidated in terms of atomic potentials. A combination of the excluded-volume effect and the local charge neutrality plays a key role in forming a structured network of $Ge(Se_{1/2})_4$ tetrahedra. The conditional packing of these basic units gives rise to the FSDP. The HNC theory revealed that the medium-range order is attenuated by the increase in the density and this causes the anomalous temperature dependence of the FSDP. We have examined thermal expansion through the shifts of the peaks in the static structure factor and have been able to distinguish the medium-range order from short-range correlations. The discrepancy between the HNC and experimental results for the position of the FSDP has been shown to be due to three-body covalent forces; these forces modify the correlations responsible for the FSDP, bringing it in quantitative agreement with experiments.[4,6]

The HNC theory works well in describing the thermodynamic and structural properties of molten and vitreous $GeSe_2$ and thus gives us confidence in applying it to the study of structural properties and phase relations in the ternary system Ag/Ge/Se.

ACKNOWLEDGMENTS

This work was supported by the U.S. Department of Energy (Division of the Office of Basic Energy Sciences) under Contract No. W-31-109-ENG-38. We would like to acknowledge a grant of computer time on Energy Research Cray computers at the National Magnetic Fusion Energy Computing Center (Livermore, CA).

*On leave from Department of Physics, University of Tokyo, Bunkyo-ku, Tokyo 113, Japan.

†Permanent address: Concurrent Computing Laboratory for Materials Simulations, Nicholson Hall, Louisiana State University, Baton Rouge, LA 70803-4001.

[1]P. H. Fuoss, P. Eisenberger, W. K. Warburton, and A. Bienenstock, Phys. Rev. Lett. **46**, 1537 (1981).

[2]A. Feltz, M. Pohle, H. Steile, and G. Helms, J. Non-Cryst. Solids **69**, 271 (1985).

[3]P. H. Fuoss and A. Fischer-Colbrie, Phys. Rev. B **38**, 1875 (1988).

[4]O. Uemura, Y. Sagara, and T. Satow, Phys. Status Solidi A **32**, K91 (1975); O. Uemura, Y. Sagara, D. Muno, and T. Satow, J. Non-Cryst. Solids **30**, 155 (1978).

[5]R. J. Nemanich, F. L. Galeener, J. C. Mikkelsen, G. A. N. Connell, G. Etherington, A. C. Wright, and R. N. Sinclair, Physica B **117-118**, 959 (1983).

[6]S. Susman, D. L. Price, K. J. Volin, and R. J. Dejus, J. Non-Cryst. Solids **106**, 26 (1988); S. Susman, D. L. Price, K. J. Volin, and D. G. Montague (unpublished).

[7]S. C. Moss and D. L. Price, in *Physics of Disordered Materials*, edited by D. Adler, H. Fritzsche, and S. R. Ovshinsky (Plenum, New York, 1985), p. 77.

[8]D. L. Price, S. C. Moss, R. Reijers, M.-L. Saboungi, and S. Susman, J. Phys. C **21**, L1069 (1988).

[9]J. C. Phillips, J. Non-Cryst. Solids **43**, 37 (1981).

[10]P. Vashishta, R. K. Kalia, and I. Ebbsjö, Phys. Rev. B **39**, 6034 (1989).

[11]P. Vashishta, R. K. Kalia, G. A. Antonio, and I. Ebbsjö, Phys. Rev. Lett. **62**, 1651 (1989).

[12]F. H. Stillinger and T. A. Weber, Phys. Rev. B **31**, 5262 (1985).

[13]R. Biswas and D. R. Hamann, Phys. Rev. Lett. **55**, 2001 (1985); R. Biswas and D. R. Hamann, Phys. Rev. B **36**, 6434 (1987).

[14]J. K. Percus and G. J. Yevick, Phys. Rev. **110**, 1 (1957).

[15]J. M. J. Van Leeuwen, J. Groeneveld, and J. De Boer, Physica **25**, 792 (1959).

[16]T. Morita, Prog. Theor. Phys. **23**, 829 (1960).

[17]H. Iyetomi, Prog. Theor. Phys. **71**, 427 (1984).

[18]H. Iyetomi, P. Vashishta, and R. K. Kalia (unpublished).

[19]H. Iyetomi, P. Vashishta, and R. K. Kalia, J. Non-Cryst. Solids **106**, 321 (1988).

[20]H. Iyetomi, P. Vashishta, and R. K. Kalia, J. Phys.: Condens. Matter **1**, 2103 (1989).

[21]Von G. Dittmar and H. Schäfer, Acta Crystallogr. B **32**, 2726 (1976).

[22]J. P. Hansen and I. R. McDonald, *Theory of Simple Liquids*, 2nd ed. (Academic, New York, 1986).

[23]S. Ichimaru, H. Iyetomi, and S. Tanaka, Phys. Rep. **149**, 91 (1987).

[24]J. A. Barker and D. Henderson, Rev. Mod. Phys. **48**, 587 (1976).

[25]M. Baus and J. P. Hansen, Phys. Rep. **59**, 1 (1980).

[26]M. Wertheim, Phys. Rev. Lett. **8**, 321 (1963).

[27]E. Thiele, J. Chem. Phys. **38**, 1959 (1963).

[28]J. L. Lebowitz, Phys. Rev. **133**, 895 (1964).

[29]N. W. Ashcroft and D. C. Langreth, Phys. Rev. **156**, 685 (1967); **166**, 934(E) (1968).

[30]J. E. Enderby and D. M. North, Phys. Chem. Liq. **1**, 1 (1968).

[31]K. Hiroike, J. Phys. Soc. Jpn. **27**, 1415 (1969).

[32]M. J. Gillan, Mol. Phys. **38**, 1781 (1979); G. M. Abernethy and M. J. Gillan, *ibid.* **39**, 839 (1980).

[33]E. Enciso, Mol. Phys. **56**, 129 (1985); E. Enciso, F. Lado, M. Lombardero, J. L. F. Abascal, and S. Lago, J. Chem. Phys. **87**, 2249 (1987).

[34]K.-C. Ng, J. Chem. Phys. **61**, 2680 (1974).

[35]F. Lado, J. Comput. Phys. **8**, 417 (1971).

[36]R. W. Johnson, D. L. Price, S. Susman, M. Arai, T. I. Morrison, and G. K. Shenoy, J. Non-Cryst. Solids **83**, 251 (1986).

[37]H. Isper, M. Gambino, and W. Schuster, Monatsh. Chem. **113**, 389 (1982).

[38]S. C. Moss, *Proceedings of the Fifth International Conference on Amorphous and Liquid Semiconductors* (Taylor and Francis, London, 1974), p. 17.

[39]M. Dixon and R. M. Atwood, Phys. Chem. Liq. **6**, 189 (1977).

[40]K. Tanaka, J. Non-Cryst. Solids **90**, 363 (1987).

[41]L. E. Busse and S. R. Nagel, Phys. Rev. Lett. **47**, 1848 (1981).

[42]H. Iyetomi and P. Vashishta, Phys. Rev. A **40**, 305 (1989).

[43]P. N. Sen and M. F. Thorpe, Phys. Rev. B **15**, 4030 (1977).